Chemical Engineering Journal 405 (2021) 126678

Contents lists available at ScienceDirect

Chemical Engineering Journal

journal homepage: www.elsevier.com/locate/cej

# High moisture resistance of an efficient $Mn^{4+}$-activated red phosphor $Cs_2NbOF_5:Mn^{4+}$ for WLEDs

Jianbang Zhou[a], Yingyuan Chen[a], Chunyan Jiang[a], Bojana Milićević[a], Maxim S. Molokeev[b,c,d], Mikhail G. Brik[e,f,g], Ivan A. Bobrikov[h], Jing Yan[i], Junhao Li[a], Mingmei Wu[a,*]

[a] School of Marine Sciences/School of Chemistry, Sun Yat-Sen University, Zhuhai 519082, Guangzhou 510275, PR China
[b] Laboratory of Crystal Physics, Kirensky Institute of Physics, Federal Research Center KSC SB RAS, Krasnoyarsk 660036, Russia
[c] Siberian Federal University, Krasnoyarsk 660041, Russia
[d] Department of Physics, Far Eastern State Transport University, Khabarovsk 680021, Russia
[e] College of Sciences, Chongqing University of Posts and Telecommunications, Chongqing 400065, PR China
[f] Institute of Physics, University of Tartu, W. Ostwald Str. 1, Tartu 50411, Estonia
[g] Institute of Physics, Jan Dlugosz University, Armii Krajowej 13/15, PL-42200 Czestochowa, Poland
[h] Frank Laboratory of Neutron Physics, Joint Institute for Nuclear Research, Dubna 141980, Russia
[i] Guangdong Institute of Semiconductor Industrial Technology, Guangzhou 510650, PR China

## HIGHLIGHTS

- $Cs_2NbOF_5:Mn^{4+}$ shows much better moisture resistance than fluoride red phosphor.
- $Nb^{5+}$ is proved to play a leading role in improving the water-resistant properties.
- The water resistance of $Mn^{4+}$-activated fluorides can be improved by $Nb^{5+}$.
- Warm WLEDs with high luminous efficacy of 174 lm/W have been fabricated.

## GRAPHICAL ABSTRACT

$Nb^{5+}$ is proved to play a major role in improving the moisture-resistant performance of $Mn^{4+}$ by self-suppressing the hydrolysis of $[MnF_6]^{2-}$ groups, which may provide a new approach to substantially improve the waterproof stability of $Mn^{4+}$-activated (oxy)fluoride red phosphors.

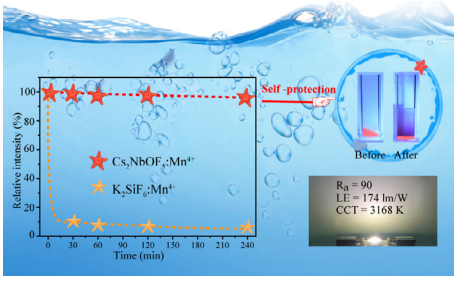


## ARTICLE INFO

*Keywords:*
Light-emitting diodes
Moisture resistance
$Mn^{4+}$
Self-protection
Photoluminescence

## ABSTRACT

$Mn^{4+}$-activated fluoride red phosphors, the most important red phosphors for warm white light emitting diodes (LEDs), usually suffer from inherent poor moisture resistance which is a major obstacle to their long-lasting outdoor applications in a high humidity environment. Surface modification of phosphors by coating with either organic or inorganic shells is an effective way to improve waterproof stability. However, the coating procedure usually has a negative impact on the luminous efficacy due to the increased passivation shell thickness. In this work, $Mn^{4+}$-activated oxyfluoroniobate ($Cs_2NbOF_5$), a highly efficient phosphor with internal quantum efficiency of *ca*. 82%, has been successfully synthesized and it is interesting to note that $Cs_2NbOF_5:Mn^{4+}$ can exhibit remarkably improved waterproof stability even without surface coating compared to well-accepted commercial fluoride red-emitting phosphor, $K_2SiF_6:Mn^{4+}$. The results obtained indicate that $Nb^{5+}$ ions inside red phosphor play a crucial role in improving the water-resistant performance of $Mn^{4+}$, which provides a new concept for overcoming the downside of their waterproof in humid conditions and maintaining the luminescence efficiency. In the final phase white LEDs with a high luminous efficacy of 174 lm/W (higher than commercial fluoride red

* Corresponding author.
*E-mail address:* ceswmm@mail.sysu.edu.cn (M. Wu).

https://doi.org/10.1016/j.cej.2020.126678
Received 3 June 2020; Received in revised form 11 August 2020; Accepted 13 August 2020
Available online 16 August 2020
1385-8947/ 

phosphors), low correlated color temperature (3164 K) and high color rendering index ($R_a$ = 90 and $R_9$ = 85) have been fabricated using $Cs_2NbOF_5:Mn^{4+}$.

## 1. Introduction

All the optical features of $Mn^{4+}$ in fluorides satisfy the requirements of a consummate red-emitting phosphor for white LEDs [1–3]. $Mn^{4+}$-activated fluoride phosphors, with narrow band emissions at ca. 630 nm and broad excitation band at *ca*. 460 nm, can be directly excited by the InGaN blue diode chip [4–9], which confirms that they are one of the most important red phosphors for improving the color rendering index (CRI) and lowering correlated color temperature (CCT) of YAG:$Ce^{3+}$ based white LEDs [10–13]. In this regard, $K_2SiF_6:Mn^{4+}$ and $K_2TiF_6:Mn^{4+}$ have already been commercialized due to their simplicity of processing and high photoluminescence (PL) quantum efficiency. However, most of these fluoride phosphors suffer from inherent poor moisture resistance as $[MnF_6]^{2-}$ on the phosphor surface can be easily hydrolyzed into dark Mn oxides and hydroxides in humid environment [14], leading to a weakened red emission intensity and deterioration of white LEDs during long-term operation. Therefore, the next challenge is to considerably improve the moisture resistance of $Mn^{4+}$ activated red phosphors [14–17].

Surface modification by coating with either organic or inorganic shell is the usual way to achieve this goal [18–21]. For instance, Liu's group [22] has successfully minimized the moisture sensitivity of $K_2SiF_6:Mn^{4+}$ by coating an alkyl phosphate layer on its surface. So did Zhang's group by coating a super-hydrophobic octadecyltrimethoxysilane shell on $K_2TiF_6:Mn^{4+}$ [23]. However, the heterogeneous organic shells may be unstable under certain conditions such as high temperature or contact with organic solvents [24]. In addition, surface organic functional groups will inevitably weaken the luminescent efficiency of phosphors. Recently, a new strategy to improve moisture resistance of fluoride red phosphors has been proposed by coating a homogeneous passive shell on either $K_2SiF_6:Mn^{4+}$ or $K_2TiF_6:Mn^{4+}$ surface using a surface-reduction [25–27] or reverse cation exchange [24] method. However, the implementation of these strategies is still unsatisfying for white LEDs with high luminous efficiency even if they improve moisture-resistant property of red phosphors. Strictly speaking, the PL intensity of red phosphors usually shows an obvious decrease during the moisture resistance test, and there is always a decrease in the PL intensity after coating compared to the original one. Thus, a new strategy to substantially improve the water-resistant property of $Mn^{4+}$ while maintaining a high luminescence efficiency is absolutely essential.

Recently, $Mn^{4+}$-activated oxyfluorides have drawn attention owing to distorted octahedral coordination and mix of ligands ($O^{2-}$ and $F^-$) which may have an intriguing influence on the phosphor features [28,29]. It was found that non-equivalent doping of $Mn^{4+}$ in some oxyfluorides may be an efficient strategy for developing new red phosphors, for example, $Cs_2NbOF_5:Mn^{4+}$ oxyfluoride exhibits excellent luminescence properties (with an excitation at ca. 465 nm and emission at *ca*. 635 nm), good thermal and color stability [30,31]. However, the crystal structure and optimized synthesis to enhance the luminescence properties of $Cs_2NbOF_5:Mn^{4+}$ need to be further analyzed. For example, β-$Cs_2NbOF_5$ shows the luminous efficacy (LE) of WLED only 90.72 lm/W and no details on moisture resistance of $Mn^{4+}$ have been addressed [30]. Therefore, water resistance as a crucial feature of the phosphors used in warm white LEDs remains an open question [30,31]. In order to study the waterproof properties of $Mn^{4+}$-activated oxyfluorides, α-$Cs_2NbOF_5:Mn^{4+}$ has been synthesized with a facile co-precipitation method and the waterproof performance without additional surface coating has been analyzed in detail under controlled humidity conditions. It has been confirmed that even without additional surface coating, the α-$Cs_2NbOF_5:Mn^{4+}$ (hereinafter referred to as $Cs_2NbOF_5:Mn^{4+}$) exhibits much better moisture resistance than the commercial fluoride red phosphor, $K_2SiF_6:Mn^{4+}$, therefore a potential mechanism has been explored.

## 2. Experimental section

### 2.1. Reagents

Hydrofluoric acid (HF, 40 wt%), CsF (99.9%), KF (99.9%), $Nb_2O_5$ (99.99%), $KMnO_4$ (99.5%), $KHF_2$ (99.0%) and hydrogen peroxide solution ($H_2O_2$, 30 wt%).

1.00 mol $L^{-1}$ of $H_2NbF_7$ solution was prepared by dissolving 13.29 g of $Nb_2O_5$ to 100 ml of HF solution (40 wt%) under heating until a clear solution was formed.

The $K_2MnF_6$ precursor was prepared by precipitation method. $KHF_2$ (9.0 g) and $KMnO_4$ (0.45 g) were dissolved in 30 ml of HF solution. Then, $H_2O_2$ (0.45 ml) was added dropwise to the solution under vigorous stirring. The deep-purple solution gradually turned to light purple and the addition was finally stopped as soon as the solution became light brown. After decanting, washing with acetone and HF three times and drying at 75 °C for 2 h, a bright yellow $K_2MnF_6$ powder was obtained.

### 2.2. Synthesis of $Cs_2NbOF_5:Mn^{4+}$ red phosphors

The schematic diagram for the synthesis of $Cs_2NbOF_5:Mn^{4+}$ is given in Fig. S1. In a typical procedure, 1.90 ml of $H_2NbF_7$ solution (1.00 mol $L^{-1}$) and 0.0247 g $K_2MnF_6$ were added to 2.50 ml of HF solution under stirring. After $K_2MnF_6$ was completely dissolved, 7.2914 g CsF was added to the solution and stirred for another 20 min. Then the HF solution was poured out, and the yellow precipitates washed with ethanol three times to remove the impurity. Finally, the collected products were dried at 70 °C for 3 h and $Cs_2NbOF_5:Mn^{4+}$ red phosphor was successfully obtained. $Cs_2NbOF_5:Mn^{4+}$ (5.0 at.% of the nominal concentration of [Mn] inside feedstocks) with a different mole ratio of CsF:$H_2NbF_7$ from 1:1 to 32:1 is used to determine the optimal synthesis condition.

### 2.3. Synthesis of $K_2NbF_7:Mn^{4+}$ red phosphors

6.00 ml of $H_2NbF_7$ solution (1.00 mol $L^{-1}$) and 0.0890 g $K_2MnF_6$ were added to 8.00 ml of HF solution under stirring. After $K_2MnF_6$ was completely dissolved, 1.0458 g KF was added to the solution and stirred for another 20 min. Then the HF solution was poured out, and the yellow precipitates were washed with ethanol three times to remove the impurity. Finally, the collected products were dried at 70 °C for 3 h and $K_2NbF_7:Mn^{4+}$ (5.0 at.%) red phosphor was successfully obtained.

### 2.4. The crystal structure of $Cs_2NbOF_5$

All peaks were indexed by a trigonal cell (*P*-3 *m*1) with parameters similar to $Cs_2NbF_6$ [32]. This structure was therefore taken as starting model for Rietveld refinement. Site of F ion was occupied by F/O ions with fixed occupations p = 0.833 and p = 0.167, respectively.

### 2.5. LED fabrication and performance measurement

LEDs with different correlated color temperatures (CCTs) were fabricated by combining blue-chip (450–460 nm, 3.0 V, 300 mA), YAG:$Ce^{3+}$ yellow phosphor and different weights of the as prepared

$Cs_2NbOF_5:Mn^{4+}$ red phosphor. The phosphors were thoroughly mixed with silicone, and the resulting phosphor-silicone mixture was coated on the blue chips. The LEDs were operated and tested at 3.0 V and at different drive currents. The photoelectric properties of the fabricated devices were measured by an auto-temperature LED optoelectronic analyzer (ATA-1000, Everfine).

### 2.6. Measurements and characterizations

The room temperature excitation and emission spectra as well as PL decays were measured with an Edinburgh Instrument FLS920 spectrometer equipped with both 450 W xenon lamp and 60 W μs flash lamp as an excitation source. The absorption and diffuse reflectance spectra were recorded from a Cary 5000 UV–vis-NIR spectrophotometer equipped with a Cary diffuse reflectance accessory, using $BaSO_4$ as the standard reference. The quantum yield was obtained from a Hamamatsu C9920-03G absolute quantum yield measurement system. Compositional analyses were verified by inductively coupled plasma-atomic emission spectrometry (ICP). The morphology of the samples was examined by a scanning electron microscope (SEM, FEI Quanta 400). The FTIR spectra in the 400–4000 $cm^{-1}$ region was examined on a spectrometer (Nicolet 330) with KBr pellets. Powder diffraction data of the $Cs_2NbOF_5$ was collected at room temperature at a range of $2\theta$ = 11–120° by Bruker D8 ADVANCE powder diffractometer (Cu-Kα radiation) and linear VANTEC detector. The step size of $2\theta$ was 0.016°, and the counting time was 1.0 s per step.

## 3. Results and discussion

### 3.1. Optimization of synthesis conditions

$Cs_2NbOF_5:Mn^{4+}$ phosphors were prepared using a co-precipitation method with different feed ratios of $CsF:H_2NbF_7$ from 1:1 to 32:1 to optimize the synthesis condition (see Experimental Section and Fig. S1 for more details). X-ray diffraction (XRD) patterns (Fig. S2) show that impurity diffraction peaks gradually disappear with increasing $CsF:H_2NbF_7$ ratio, and pure $Cs_2NbOF_5$ was formed when the ratio was above 12:1. All diffraction peaks can be indexed to the $Cs_2NbOF_5$ phase and no traces of $K_2MnF_6$ residual or other impurity phases were noted. When carefully observed, it can be seen that the relative intensity of the diffraction peaks varied with an increase in the ratio of $CsF:H_2NbF_7$ and the peak at $2\theta$ = 24° became extremely strong with a feed ratio of 24:1, indicating a high orientation of $Cs_2NbOF_5$ particles. However, the relative intensity of this peak ($2\theta$ = 24°) decreased as the ratio of $CsF:H_2NbF_7$ increased further, leading to a decrease in particle orientation. Rietveld refinement (Fig. S3) of $Cs_2NbOF_5$ was performed for the first time to confirm the exact crystal structure. It was shown that $Cs_2NbOF_5$ crystallizes in *P3m*1 space group of the trigonal crystal system (Fig. 1a and Table S1). Detailed structural determination, coordinates of atoms (Table S2) and main bond lengths (Table S3) are addressed in ESI.

When the feed ratio of $CsF:H_2NbF_7$ rises, the body color of $Cs_2NbOF_5:Mn^{4+}$ phosphors under daylight changes from dark, light yellow and finally to deep yellow (Fig. S4), suggesting an increased $Mn^{4+}$ content. The nominal concentration of [Mn] in the feedstocks was maintained at 5.0 at.% as compared to [Nb], while the actual $Mn^{4+}$ concentration in $Cs_2NbOF_5:Mn^{4+}$ phosphors with different feed ratio

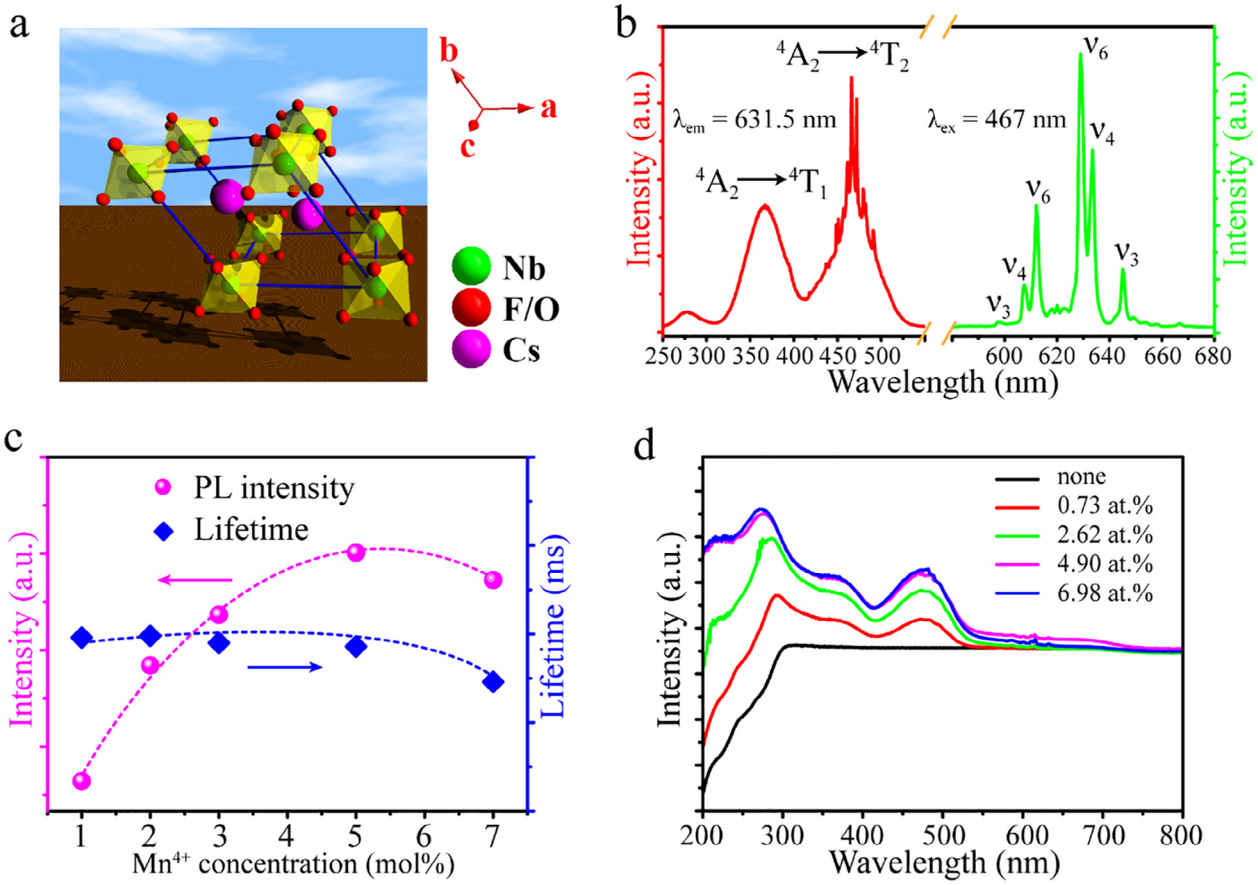


**Fig. 1.** (a) Crystal structure of $Cs_2NbOF_5$. (b) Excitation ($\lambda_{em}$ = 631.5 nm) and emission ($\lambda_{ex}$ = 467 nm) spectra of $Cs_2NbOF_5:Mn^{4+}$ (4.90 at.%). (c) PL intensity and lifetime ($\lambda_{ex}$ = 467 nm, $\lambda_{em}$ = 631.5 nm) and (d) absorption spectra of $Cs_2NbOF_5:Mn^{4+}$ as a function of $Mn^{4+}$ contents at room temperature.

was determined by ICP (Table S4). The sample synthesized with feed ratio of 24:1 ($CsF:H_2NbF_7$) was found to have the highest $Mn^{4+}$ content (4.90 at%), indicating that 98% of $Mn^{4+}$ in the solution could be successfully doped into the host lattice. This sample (24:1) demonstrates much higher emission intensity around 630 nm (Fig. 1b and Fig. S5a) and internal quantum efficiency (IQE) than the others (Table S4 and Fig. S5b). When the ratio of $CsF:H_2NbF_7$ was below 20:1, majority of $Cs_2NbOF_5:Mn^{4+}$ particles had an irregular shape with several microns in size (Fig. S6). On the other hand, the particles shaped in long bars around 100 μm when the ratio was 24:1 (Fig. S6d), which is well-aligned with the XRD results (high orientation at feed ratio of 24:1, Fig. S2). The bar-like morphology is highly related to the inherent trigonal crystal structure. A further increase in the feed ratio led to a decrease in the aspect ratio and the orientation of the micro-bars (Fig. S6e and S6f), which is also consistent with the XRD results. Considering the highest emission intensity and IQE, the optimal synthesis condition of $Cs_2NbOF_5:Mn^{4+}$ was determined to be 24:1 of $CsF:H_2NbF_7$.

### 3.2. Luminescence properties of $Cs_2NbOF_5:Mn^{4+}$

Using the optimal synthesis condition ($CsF:H_2NbF_7$ = 24:1) confirmed in the last section, a series of $Cs_2NbOF_5:Mn^{4+}$ samples were synthesized with different $Mn^{4+}$ content as determined by ICP method to be 0.00, 0.73, 1.99, 2.62, 4.90 and 6.98 at.%, respectively (Table S5). Due to a smaller ionic radius of $Mn^{4+}$ than $Nb^{5+}$, the XRD patterns shift to higher Bragg's angles (Fig. S7) with an increase of $Mn^{4+}$ content as expected, indicating successful doping of $Mn^{4+}$ into the $Cs_2NbOF_5$ host lattice.

Fig. 1b illustrates the excitation and emission spectra of $Cs_2NbOF_5:Mn^{4+}$ at room temperature. In accordance with the previously reported results of $Mn^{4+}$-activated fluorides, there are two intense excitation bands in 310 – 525 nm wavelength range, corresponding to the spin-allowed transitions of $^4A_2 \rightarrow {}^4T_1$ (366 nm) and $^4A_2 \rightarrow {}^4T_2$ (467 nm), respectively. The charge transfer transition between $F^-$ and $Mn^{4+}$ ions results in the excitation band from 250 nm to 300 nm [10]. The red emission attributed to the spin-forbidden $^2E_g \rightarrow {}^4A_2$ transition includes several sharp lines at 600.5, 610.5, 615.5, 631.5, 636.5, and 648 nm, originating from the transitions of anti-Stokes $v_3(t_{1u})$, $v_4(t_{1u})$, and $v_6(t_{2u})$ and Stokes $v_6(t_{2u})$, $v_4(t_{1u})$, and $v_3(t_{1u})$ vibronic modes, respectively, which is typical red emission of $Mn^{4+}$-activated fluorides [33]. The emission feature of the $Mn^{4+}$ ions doped oxyfluoride with negligible red-shift is almost identical to those of $Mn^{4+}$-activated fluorides.

For the first time, the energy levels of $Mn^{4+}$ ions in $Cs_2NbOF_5$ were calculated using the exchange charge model of crystal field. All calculation details can be found in our previous work [34–38]. The correlation between calculated $Mn^{4+}$ energy levels and experimental excitation/emission spectra is shown in Fig. S8. Well-alignment between the calculated energy levels (Table S6) and experimental data was obtained when the Racah parameters $B$ and $C$ are 545 $cm^{-1}$ and 3965 $cm^{-1}$, respectively. The point symmetry of the Nb site occupied by $Mn^{4+}$ is trigonal, which is reflected in the calculated crystal field parameters. Herein, non-zero parameters (in Stevens normalization, $cm^{-1}$) of $B_2^0$ = –1351.5, $B_4^0$ = –3540.4 and $B_4^3$ = 107808.4 are typical for the trigonal crystal field.

Maximum values of PL intensity (Fig. 1b) and external quantum efficiency (EQE, Table S5) of $Cs_2NbOF_5:Mn^{4+}$ are obtained with a $Mn^{4+}$ content of 4.90 at.%. The lifetime values of $Cs_2NbOF_5:Mn^{4+}$ are almost the same if the $Mn^{4+}$ content is below 4.90 at.% (3.43–3.48 ms) compared to the decreased value at 6.98 at.% (3.23 ms), as shown in Fig. 1c and Fig. S9. Therefore, concentration quenching occurs when the $Mn^{4+}$ content exceeds 4.90 at.%, which is well-aligned with PL data. IQE reaches a maximum value (81.7%) with a $Mn^{4+}$ content of 2.62 at.% (Table S5), while the absorption efficiency rises with

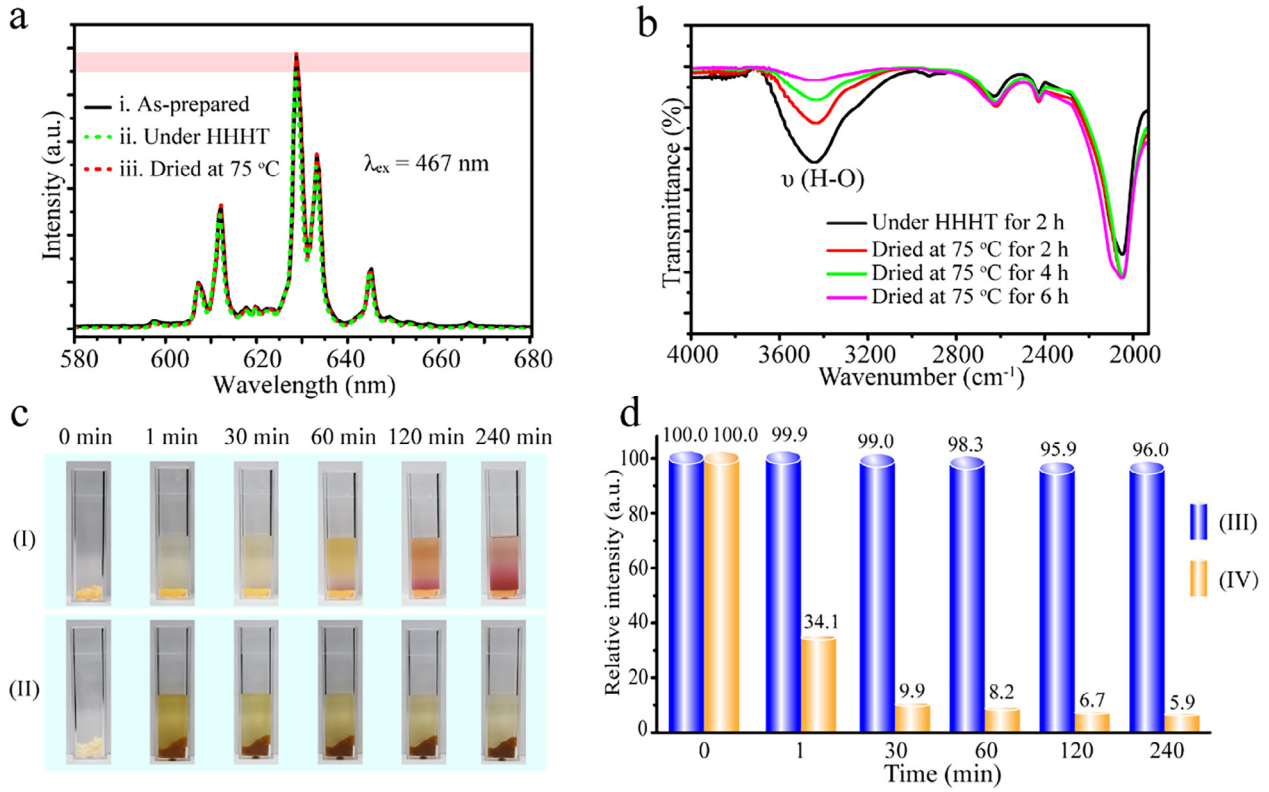


**Fig. 2.** (a) The emission spectra of $Cs_2NbOF_5:Mn^{4+}$: (i) as-prepared, (ii) aging under high humidity atmosphere (HH 85%) and high temperature (HT 85 °C) for 2 h and (iii) then dried at 75 °C for 6 h. (b) FTIR spectra of hydrated and dehydrated $Cs_2NbOF_5:Mn^{4+}$ at 75 °C for different time. (c) Photographs of $Cs_2NbOF_5:Mn^{4+}$ (I) and $K_2SiF_6:Mn^{4+}$ (II) phosphors as a function of immersion period in deionized water. (d) The relative emission intensity ($\lambda_{ex}$ = 467 nm) of $Cs_2NbOF_5:Mn^{4+}$ (III) and $K_2SiF_6:Mn^{4+}$ (IV) as a function of immersion period in deionized water.

increasing doping amount of $Mn^{4+}$ as shown in the absorption spectra (Fig. 1d). Thus, a maximum EQE value of 54.6% for $Mn^{4+}$ content of 4.90 at.% is achieved which is as high as $K_2SiF_6Mn^{4+}$ phosphor [22].

### 3.3. Improved moisture resistance

These years, $Mn^{4+}$-activated fluoride red phosphors as a kind of most promising red phosphors for white LEDs have attracted a large amount of attention, however their unique optical properties and high luminescence efficiency are extremely sensitive to moisture [27]. Avoiding surface treatment of phosphors, we have proposed a moisture resistant $Cs_2NbOF_5:Mn^{4+}$ that preserves its luminescence efficiency to a large degree in humid environment. To the best of our knowledge, the moisture-resistant property of $Mn^{4+}$-activated $Cs_2NbOF_5$ has not been reported so far.

In this work, it was found that $Cs_2NbOF_5:Mn^{4+}$ exhibits much better moisture stability than commercial $K_2SiF_6:Mn^{4+}$ red phosphor (Fig. S10). After aging under high humidity (HH 85%) and high temperature (HT 85 °C) for 2 h, the emission intensity of $Cs_2NbOF_5:Mn^{4+}$ showed only a slight decrease compared to the as-prepared one (Fig. 2a). Surprisingly, the emission intensity was recovered to its original value after dehydration at 75 °C for 6 h, as shown in curve iii of Fig. 2a. In addition, the Fourier-transform infrared (FTIR) spectra shows that the intensity of broad absorption band around 3500 $cm^{-1}$ (assigned to water molecules) decreased significantly after dehydration (Fig. 2b), indicating that most of the absorbed water molecules was removed by heating.

To further investigate the moisture-resistant property comparatively, $Cs_2NbOF_5:Mn^{4+}$ and $K_2SiF_6:Mn^{4+}$ powdery phosphors were immersed in deionized water for different periods of time (I and II of Fig. 2c). The results indicate that the yellow tint of $Cs_2NbOF_5:Mn^{4+}$ sample remained unchanged even after 240 min in water (I), whereas the yellow tint of the $K_2SiF_6:Mn^{4+}$ sample almost instantly turned into brown (II). Under blue light irradiation, $Cs_2NbOF_5:Mn^{4+}$ shows bright red emission even after 240 min in water, while $K_2SiF_6:Mn^{4+}$ has almost invisible emission to naked eyes (Fig. S10). The measured PL intensity verified that $Cs_2NbOF_5:Mn^{4+}$ retained 96.0% of its initial emission intensity after immersion in water for 240 min as shown in III of Fig. 2d (detailed emission spectra are presented in Fig. 3a and b). Under the same conditions, $K_2SiF_6:Mn^{4+}$ sample showed a significant reduction in the emission intensity (34.1%) after only 1.0 min and after 240 min its emission dropped to only 5.9% of the initial value as shown in IV of Fig. 2d (detailed emission spectra are presented in Fig. 3c and d). All these results clearly indicate that $Cs_2NbOF_5:Mn^{4+}$ red phosphor has excellent waterproof stability.

It is important to confirm why $Cs_2NbOF_5:Mn^{4+}$ has shown such a good moisture-resistant property, which may further provide a new approach to improve the moisture resistance of $Mn^{4+}$ activated fluoride red phosphors. Herein, two main hypotheses may explain the excellent moisture stability. The special structure of oxyfluorides may have some intriguing effect on the chemical stability of phosphors owing to the distorted octahedral coordination and mix-ligands of $O^{2-}$ and $F^-$ (hypothesis I). $Nb^{5+}$ played a dominant role in the improvement of the moisture-resistant property by preventing the hydrolysis of $[MnF_6]^{2-}$ group (hypothesis II). A set of experiments and measurements have

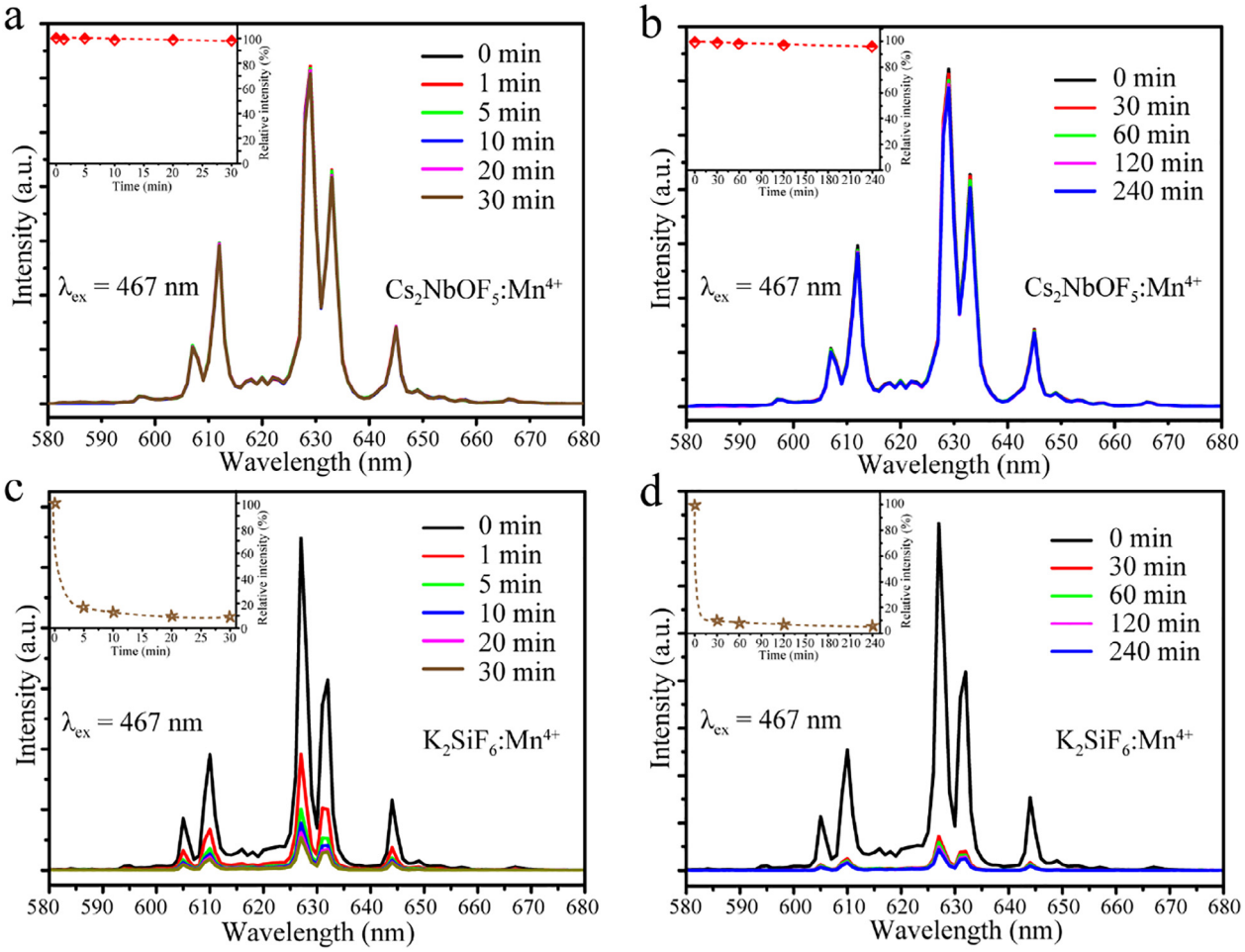


**Fig. 3.** The emission spectra of $Cs_2NbOF_5:Mn^{4+}$ (a and b) and $K_2SiF_6:Mn^{4+}$ (c and d) after immersion in deionized water for 30 and 240 min, respectively. The insets show the relative emission intensities of $Cs_2NbOF_5:Mn^{4+}$ and $K_2SiF_6:Mn^{4+}$ as a function of immersion period in deionized water.

been carried out in order to determine which one is correct. Firstly, the crystal structures of both $Cs_2NbOF_5:Mn^{4+}$ and $K_2SiF_6:Mn^{4+}$ phosphors were investigated, which did not change even after immersion in water (Fig. S11). Secondly, the diffuse reflectance spectra (DRS) of $Cs_2NbOF_5:Mn^{4+}$ and $K_2SiF_6:Mn^{4+}$ phosphors (before and after immersion in water for different periods of time) were compared in Fig. 4a and b. It was clearly confirmed that there are two characteristic absorption bands of $Mn^{4+}$ centered around 360 nm ($^4A_2 \rightarrow {}^4T_1$) and 460 nm ($^4A_2 \rightarrow {}^4T_2$) for both samples before immersion. Absorption bands (Fig. 4a) in the DRS and body color (Fig. 2c) of $Cs_2NbOF_5:Mn^{4+}$ powders remained almost unchanged even after 240 min in water, which implies that the hydrolysis of $[MnF_6]^{2-}$ into Mn oxides and hydroxides was prevented. This result is well-aligned with the excellent PL stability of $Cs_2NbOF_5:Mn^{4+}$ after immersion in water (Fig. 3a and b). On the contrary, the DRS of $K_2SiF_6:Mn^{4+}$ has changed significantly. The characteristic absorption bands of $Mn^{4+}$ disappear after 30 min, while a flat broad absorption band appears in the wavelength range from ultraviolet to visible region (Fig. 4b), suggesting the hydrolysis of $[MnF_6]^{2-}$ group and the undesirable presence of Mn oxides and hydroxides [26]. This results in darkness of the body color (II of Fig. 2c) and decrease in PL intensity of $K_2SiF_6:Mn^{4+}$ (Fig. 3c and d).

It could be observed that the colorless suspension of $Cs_2NbOF_5:Mn^{4+}$ in aqueous solution becomes purple over time, whereas the color of $K_2SiF_6:Mn^{4+}$ aqueous solution does not change (Fig. 2c). The purple color of $Cs_2NbOF_5:Mn^{4+}$ solution is unusual and could be related to its moisture resistance. In this regard, the absorption spectra of aliquots taken at different times from $Cs_2NbOF_5:Mn^{4+}$ aqueous solution are shown in Fig. 4c. A broad absorption band in the wavelength range of 410–600 nm is evident, while $K_2SiF_6:Mn^{4+}$ aqueous solution does not show any absorption peak in a separate experiment (Fig. 4d). Since the purple color is considered to be typical for the $[MnO_4]^-$ solution, the absorption spectrum of the $KMnO_4$ solution (Fig. 4c) was compared with the $Cs_2NbOF_5:Mn^{4+}$ solution, indicating well aligned absorption bands of both solutions. This result reveals that a certain amount of $Mn^{4+}$ has been oxidized to $[MnO_4]^-$ when $Cs_2NbOF_5:Mn^{4+}$ powder was immersed in water. To further establish the presence of $[MnO_4]^-$, hydrogen peroxide solution ($H_2O_2$, 30 wt%) was added drop by drop to purple $Cs_2NbOF_5:Mn^{4+}$ solution. The reaction triggered the appearance of bubbles and the purple color became colorless (Video S1), which is a typical phenomenon for $[MnO_4]^-$ solutions. The possible chemical reaction from $Mn^{4+}$ to $[MnO_4]^-$ was explored (Fig. S12). From literature [39–41], it is known that niobium as a catalyst plays an important role in the oxidation process of hydrocarbons. From the above results, it can be confirmed that the presence of $Nb^{5+}$ can improve the water-resistant performance of $Mn^{4+}$-activated phosphors (hypothesis II).

To further verify the hypothesis II, $K_2NbF_7:Mn^{4+}$, a $Mn^{4+}$ activated niobium-based fluoride (only $F^-$ ligands), was synthesized (Fig. S13a) and tested for moisture resistance. It could be observed that $K_2NbF_7:Mn^{4+}$ preserved a yellowish color during the water resistance test, indicating good chemical stability. In addition, the presence of $[MnO_4]^-$ in $K_2NbF_7:Mn^{4+}$ aqueous solution (Fig. S13b and Fig. S13c) was confirmed, the same as in $Cs_2NbOF_5:Mn^{4+}$. To draw a conclusion, the above results further confirm that $Nb^{5+}$ plays a leading role in

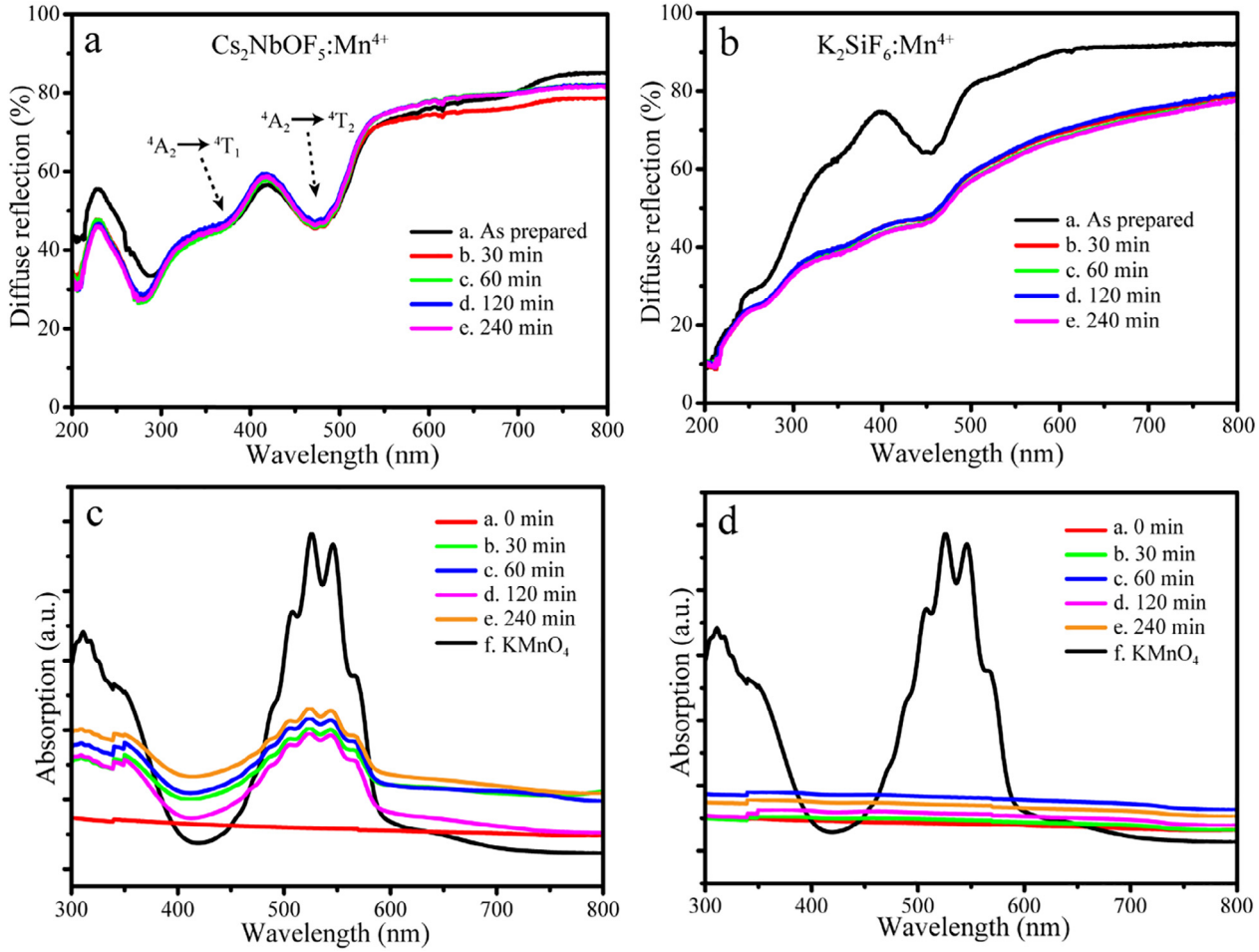


**Fig. 4.** Diffuse reflection spectra of (a) $Cs_2NbOF_5:Mn^{4+}$ and (b) $K_2SiF_6:Mn^{4+}$ phosphors before and after immersion in deionized water for different time. Absorption spectra of the suspension of (c) $Cs_2NbOF_5:Mn^{4+}$ and (d) $K_2SiF_6:Mn^{4+}$ before and after immersion in deionized water for different time, and the aqueous solution of $KMnO_4$.

improving the waterproof stability of both $Cs_2NbOF_5:Mn^{4+}$ and $K_2NbF_7:Mn^{4+}$ phosphors.

If observed carefully, the purple color (i.e. $[MnO_4]^-$) has always occurred first at the interface between solid particles and liquid water, no matter the solid particles are $Cs_2NbOF_5:Mn^{4+}$ (Fig. 2c) or $K_2NbF_7:Mn^{4+}$ (Fig. S13b). Thus, it may imply that the concentration of $Nb^{5+}$ in the solution dominated this process. To analyze the mechanism for improving the moisture resistance of $Cs_2NbOF_5:Mn^{4+}$ phosphor caused by $Nb^{5+}$, a series of solutions with different $Nb^{5+}$ contents (0.005 ~ 0.045 mol/L) were prepared while maintaining the same amount of $K_2MnF_6$ (Fig. S14). It can be observed that with a low $Nb^{5+}$ content (below 0.015 mol/L) the solution quickly becomes brown due to the hydrolysis of $[MnF_6]^{2-}$ group. With increasing $Nb^{5+}$ content (0.020 ~ 0.030 mol/L), the solution turns brown more slowly and the brown products gradually disappear, which means that the hydrolysis of $[MnF_6]^{2-}$ was completely suppressed with a high $Nb^{5+}$ content. The above results suggest that $Nb^{5+}$ may inhibit the hydrolysis of the $[MnF_6]^{2-}$ group and this effect becomes stronger as the $Nb^{5+}$ content increases.

Considering the extraordinary performance of $Nb^{5+}$ in improving the waterproof stability, this study may provide a new route to advance the water-resistant property of $Mn^{4+}$-activated fluoride red phosphors. On the basis of the hypothesis II outlined above, another simple experiment was carried out. The same amount of yellowish $K_2SiF_6:Mn^{4+}$ powders was added to aqueous solutions with different $Nb^{5+}$ content (0.000 ~ 0.050 mol/L) and aged for three months (Fig. S15). $K_2SiF_6:Mn^{4+}$ powder sample immersed in water (without $Nb^{5+}$) turns brown immediately due to the hydrolysis of $[MnF_6]^{2-}$ group. However, even at a low concentration of $Nb^{5+}$ (below 0.010 mol/L) there is only a slight change in the color of $K_2SiF_6:Mn^{4+}$ powder. Moreover, the body color of $K_2SiF_6:Mn^{4+}$ powder inside the solution remained unchanged at a high $Nb^{5+}$ content (above 0.015 mol/L) even after three months, indicating that the hydrolysis of $[MnF_6]^{2-}$ was completely suppressed by the presence of $Nb^{5+}$ (Fig. S15). This experiment shows a feasible way to significantly improve the moisture-resistant property of $Mn^{4+}$-activated fluoride red phosphors by introducing $Nb^{5+}$.

In addition, color stability under different temperature is also an important parameter of phosphors used for LED fabrication and can be described by the chromaticity shift (ΔE, for more details see Eq. S3) [42,43]. Fig. 5a demonstrates that $Cs_2NbOF_5:Mn^{4+}$ exhibits better color stability than commercial red phosphors ($CaAlSiN_3:Eu^{2+}$ and $K_2SiF_6:Mn^{4+}$) in the temperature range from 298 K to 423 K. The thermal stability of $Cs_2NbOF_5:Mn^{4+}$ from room temperature to high temperature is illustrated in Fig. S16.

### 3.4. Fabrication and performance of white LEDs

Due to the outstanding emission efficiency, moisture resistance and color stability, it is necessary to evaluate the practical application of $Cs_2NbOF_5:Mn^{4+}$ red phosphor inside white LEDs. White LEDs fabricated with only YAG:$Ce^{3+}$ show low CRI of $R_a$ = 73, $R_9$ = -45 and high CCT of 8080 K, which is not suitable for indoor lighting due to lack of red emission. By combining red $Cs_2NbOF_5:Mn^{4+}$ and yellow YAG:$Ce^{3+}$ phosphors, packaged warm white LEDs have a high CRI of $R_a$ = 90, $R_9$ = 85 and high luminous efficacy of 174 lm/W (Fig. 5b), which is higher than that of $K_2TiF_6:Mn^{4+}$ commercial fluoride red phosphor [10] (herein, $K_2TiF_6:Mn^{4+}$ was taken as a reference because of its higher luminescence efficiency than $K_2SiF_6:Mn^{4+}$) [6]. In addition, the current-dependent photoelectric parameters (Table S7) indicates that the luminous efficacy of the as-fabricated white LED at different power is much higher than that of $K_2TiF_6:Mn^{4+}$ fabricated white LED (Table S8 and Fig. S17). The chromaticity coordinates of the typical LED with CCT of 3168 K are close to the black body locus, as marked in Fig. S18. These excellent results reveal that $Cs_2NbOF_5:Mn^{4+}$ may potentially be used as a red component for white LEDs.

## 4. Conclusions

In summary, oxyfluoroniobate $Cs_2NbOF_5:Mn^{4+}$ was prepared using a co-precipitation method and the synthesis condition was optimized to achieve the highest luminescence intensity and IQE by adjusting feed ratios. The unique luminescence features of $Cs_2NbOF_5:Mn^{4+}$, including strong broadband absorption at ~ 467 nm and high-purity sharp red emission at ~ 631.5 nm, are the same as $Mn^{4+}$-activated fluoride red phosphors. Using $Cs_2NbOF_5:Mn^{4+}$ red phosphor, warm white LEDs (CCT = 3168 K and $R_a$ = 90) with high luminous efficacy of 174 lm/W were fabricated. Interestingly, it was found that $Cs_2NbOF_5:Mn^{4+}$ exhibits much better moisture resistance than commercial fluoride red phosphors. The $Cs_2NbOF_5:Mn^{4+}$ sample retained 96.0% of its original emission intensity even after immersion in water for 240 min, whereas $K_2SiF_6:Mn^{4+}$ retained only 5.9%. It was found that $Nb^{5+}$ plays a leading role in improving the moisture-resistant property of $Mn^{4+}$ by self-suppressing the hydrolysis of $[MnF_6]^{2-}$ groups. It has been confirmed that the self-inhibiting effect becomes stronger with an increase of $Nb^{5+}$ content in $K_2MnF_6$ solution. The results revealed a feasible way to substantially improve the moisture-resistant property of $Mn^{4+}$-activated fluoride red phosphors by introducing $Nb^{5+}$, which opens up a new avenue for the development of high waterproof $Mn^{4+}$-activated red-emitting phosphors using self-protective elements.

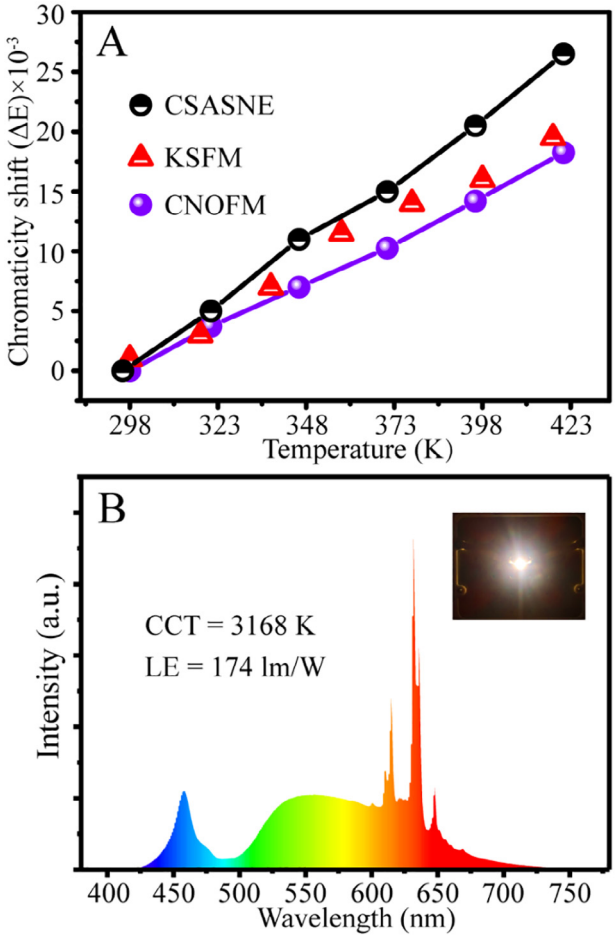


**Fig. 5.** (a) Chromaticity shift of $Cs_2NbOF_5:Mn^{4+}$, $CaAlSiN_3:Eu^{2+}$ (CSASNE) and $K_2SiF_6:Mn^{4+}$ (KSFM) in the temperature range from 298 K to 423 K. (b) Electroluminescent spectra of a fabricated white LED using $Cs_2NbOF_5:Mn^{4+}$ red phosphor with CCT of 3168 K. The inset shows photograph of the as-prepared white LED. (For interpretation of the references to color in this figure legend, the reader is referred to the web version of this article.)

## Declaration of Competing Interest

The authors declare that they have no known competing financial interests or personal relationships that could have appeared to influence the work reported in this paper.

## Acknowledgements

This work was financially supported by grants from the National Natural Science Foundation of China (No. 51802359, 21801254, 51902354) and its Joint Funds of Yunnan and Guangdong Province (No. U1702254 and No. U1801253), Special Fund of Guangdong Province Project for Applied Science and Technology Research and Development (No. 2017B090917001), Guangdong Basic and Applied Basic Research Foundation (No. 2020A1515010556), the Fundamental Research Funds for the Central Universities (No. 19lgpy123), and China Postdoctoral Science Foundation (No. 2019M663230). M. G. Brik thanks the supports from the National Recruitment Program of High-end Foreign Experts (No. GDT20185200479 and GDW20145200225), the Programme for the Foreign Experts (No. W2017011) and Wenfeng High-end Talents Project (No. W2016-01) offered by Chongqing University of Posts and Telecommunications (CQUPT), Estonian Research Council grant PUT PRG111, and European Regional Development Fund (TK141).

## Appendix A. Supplementary data

Supplementary data to this article can be found online at https://doi.org/10.1016/j.cej.2020.126678.

## References

[1] T. Senden, R.J.A. van Dijk-Moes, A. Meijerink, Quenching of the red $Mn^{4+}$ luminescence in $Mn^{4+}$-doped fluoride LED phosphors, Light Sci. Appl. 7 (2018) 74–86.
[2] M. Kim, W.B. Park, J.W. Lee, J. Lee, C.H. Kim, S.P. Singh, K.S. Sohn, $Rb_3SiF_7:Mn^{4+}$ and $Rb_2CsSiF_7:Mn^{4+}$ red-emitting phosphors with a faster decay rate, Chem. Mater. 30 (2018) 6936–6944.
[3] R. Verstraete, H.F. Sijbom, J.J. Joos, K. Korthout, D. Poelman, C. Detavernier, P.F. Smet, Red $Mn^{4+}$-doped fluoride phosphors: why purity matters, ACS Appl. Mater. Interfaces 10 (2018) 18845–18856.
[4] Z.G. Xia, Q.L. Liu, Progress in discovery and structural design of color conversion phosphors for LEDs, Prog. Mater Sci. 84 (2016) 59–117.
[5] Z. Zhou, N. Zhou, M. Xia, M. Yokoyama, H.T. Hintzen, Research progress and application prospects of transition metal $Mn^{4+}$-activated luminescent materials, J. Mater. Chem. C 4 (2016) 9143–9161.
[6] H.D. Nguyen, R.S. Liu, Narrow-band red-emitting $Mn^{4+}$-doped hexafluoride phosphors: synthesis, optoelectronic properties, and applications in white light-emitting diodes, J. Mater. Chem. C 4 (2016) 10759–10775.
[7] D.Q. Chen, Y. Zhou, J.S. Zhong, A review on $Mn^{4+}$ activators in solids for warm white light-emitting diodes, RSC Adv. 6 (2016) 86285–86296.
[8] C.C. Lin, A. Meijerink, R.S. Liu, Critical red components for next-generation white LEDs, J. Phys. Chem. Lett. 7 (2016) 495–503.
[9] J.H. Li, J. Yan, D.W. Wen, W.U. Khan, J.X. Shi, M.M. Wu, Q. Su, P.A. Tanner, Advanced red phosphors for white light-emitting diodes, J. Mater. Chem. C 4 (2016) 8611–8623.
[10] H.M. Zhu, C.C. Lin, W.Q. Luo, S.T. Shu, Z.G. Liu, Y.S. Liu, J.T. Kong, E. Ma, Y.G. Cao, R.S. Liu, X.Y. Chen, Highly efficient non-rare-earth red emitting phosphor for warm white light-emitting diodes, Nat. Commun. 5 (2014) No.4312.
[11] W.L. Zhou, M.H. Fang, S.X. Lian, R.S. Liu, Ultrafast self-crystallization of high-external-quantum-efficient fluoride phosphors for warm white light-emitting diodes, ACS Appl. Mater. Interfaces 10 (2018) 17508–17511.
[12] W.L. Zhou, R.H. Wang, L.C. Yin, J. Chen, C.C. Su, X.R. Xing, R.S. Liu, Alcohol-guided growth of two-dimensional narrow-band red-emitting $K_2TiF_6:Mn^{4+}$ for white-light-emitting diodes, ACS Appl. Mater. Interfaces 11 (2019) 20143–20149.
[13] W.L. Wu, M.H. Fang, W.L. Zhou, T. Lesniewski, S. Mahlik, M. Grinberg, M.G. Brik, H.S. Sheu, B.M. Cheng, J. Wang, R.S. Liu, High color rendering index of $Rb_2GeF_6:Mn^{4+}$ for light-emitting diodes, Chem. Mater. 29 (2017) 935–939.
[14] L. Huang, Y. Liu, S.C. Si, M.G. Brik, C.X. Wang, J. Wang, A new reductive DL-mandelic acid loading approach for moisture-stable $Mn^{4+}$ doped fluorides, Chem. Commun. 54 (2018) 11857–11860.
[15] C.Y. Jiang, L.H. Li, M.G. Brik, L.T. Lin, M.Y. Peng, Epitaxial growth via anti-solvent-induced deposition towards a highly efficient and stable $Mn^{4+}$ doped fluoride red phosphor for application in warm WLED, J. Mater. Chem. C 7 (2019) 6077–6084.
[16] Y. Liu, Z. Zhou, L. Huang, M.G. Brik, S.C. Si, L.T. Lin, T.T. Xuan, H.B. Liang, J.B. Qiu, J. Wang, High-performance and moisture-resistant red-emitting $Cs_2SiF_6:Mn^{4+}$ for high-brightness LED backlighting, J. Mater. Chem. C 7 (2019) 2401–2407.
[17] M.H. Fang, C.S. Hsu, C.C. Su, W.J. Liu, Y.H. Wang, R.S. Liu, Integrated surface modification to enhance the luminescence properties of $K_2TiF_6:Mn^{4+}$ phosphor and its application in white-light-emitting diodes, ACS Appl. Mater. Interfaces 10 (2018) 29233–29237.
[18] F. Hong, H.P. Xu, G. Pang, G.X. Liu, X.T. Dong, W.S. Yu, Moisture resistance, luminescence enhancement, energy transfer and tunable color of novel core-shell structure $BaGeF_6:Mn^{4+}$ phosphor, Chem. Eng. J. 390 (2020) 124579.
[19] Y.X. Liu, J.X. Xu, L.C. Ju, C. Cai, V.B. Hao, S.H. Zhang, Z.W. Zhang, X. Xu, X. Jian, L.J. Yin, Hydrophobic surface modification toward highly stable $K_2SiF_6:Mn^{4+}$ phosphor for white light-emitting diodes, Ceram. Int. 46 (2020) 8811–8818.
[20] B. Zhang, J.W. Wang, L.Y. Hao, X. Xu, S. Agathopoulos, L.J. Yin, C.M. Wang, H.T. (Bert) Hintzen, Highly stable red-emitting $Sr_2Si_5N_8:Eu^{2+}$ phosphor with a hydrophobic surface, J. Am. Ceram. Soc. 100 (2017) 257–264.
[21] B. Zhang, J.W. Zhang, H. Zhong, L.Y. Hao, X. Xu, S. Agathopoulos, C.M. Wang, L.J. Yin, Highly stable modified phosphors of $Ba_2SiO_4:Eu^{2+}$ by forming a robust hydrophobic inorganic surface layer of Silicon-Oxy-Imide-Carbide, J. Phys. Chem. C 121 (2017) 11616–11622.
[22] H.D. Nguyen, C.C. Lin, R.S. Liu, Waterproof alkyl phosphate coated fluoride phosphors for optoelectronic materials, Angew. Chem. Int. Ed. 54 (2015) 10862–10866.
[23] Y.Y. Zhou, E.H. Song, T.T. Deng, Q.Y. Zhang, Waterproof narrow-band fluoride red phosphor $K_2TiF_6:Mn^{4+}$ via facile superhydrophobic surface modification, ACS Appl. Mater. Interfaces 10 (2018) 880–889.
[24] D.C. Huang, H.M. Zhu, Z.H. Deng, Q.L. Zou, H.Y. Lu, X.D. Yi, W. Guo, C.Z. Lu, X.Y. Chen, Moisture-resistant $Mn^{4+}$-doped core-shell structured fluoride red phosphor exhibiting high luminous efficacy for warm white LEDs, Angew. Chem. Int. Ed. 58 (2019) 3843–3847.
[25] C.Y. Jiang, M.G. Brik, A.M. Srivastava, L.H. Li, M.Y. Peng, Significantly conquering moisture-induced luminescence quenching of red line-emitting phosphor $Rb_2SnF_6:Mn^{4+}$ through $H_2C_2O_4$ triggered particle surface reduction for blue converted warm white light-emitting diodes, J. Mater. Chem. C 7 (2019) 247–255.
[26] L. Huang, Y. Liu, J.B. Yu, Y.W. Zhu, F.J. Pan, T.T. Xuan, M.G. Brik, C.X. Wang, J. Wang, Highly stable $K_2SiF_6:Mn^{4+}@K_2SiF_6$ composite phosphor with narrow red emission for white LEDs, ACS Appl. Mater. Interfaces 10 (2018) 18082–18092.
[27] Y.Y. Zhou, E.H. Song, T.T. Deng, Y.J. Wang, Z.G. Xia, Q.Y. Zhang, Surface passivation toward highly stable $Mn^{4+}$-activated red-emitting fluoride phosphors and enhanced photostability for white LEDs, Adv. Mater. Interfaces 6 (2019) 1802006.
[28] T. Hu, H. Lin, Y. Cheng, Q.M. Huang, J. Xu, Y. Gao, J.M. Wang, Y.S. Wang, A highly-distorted octahedron with a C-2v group symmetry inducing an ultra-intense zero phonon line in $Mn^{4+}$-activated oxyfluoride $Na_2WO_2F_4$, J. Mater. Chem. C 5 (2017) 10524–10532.
[29] Y. Zhou, S. Zhang, X.M. Wang, H. Jiao, Structure and luminescence properties of $Mn^{4+}$-activated $K_3TaO_2F_4$ red phosphor for white LEDs, Inorg. Chem. 58 (2019) 4412–4419.
[30] H. Ming, J.F. Zhang, L.L. Liu, J.Q. Peng, F. Du, X.Y. Ye, Y.M. Yang, H.P. Nie, A novel $Cs_2NbOF_5:Mn^{4+}$ oxyfluoride red phosphor for light-emitting diode devices, Dalton Tran. 47 (2018) 16048–16056.
[31] Q. Wang, Z.Y. Yang, H.Y. Wang, Z.K. Chen, H.L. Yang, J. Yang, Z.L. Wang, Novel $Mn^{4+}$-activated oxyfluoride $Cs_2NbOF_5:Mn^{4+}$ red phosphor for warm white light-emitting diodes, Opt. Mater. 85 (2018) 96–99.
[32] J. Chassaing, M.B. de Bournonville, D. Bizot, M. Quarton, Structural and magnetic studies of $Rb_2NbF_6$ and $Cs_2NbF_6$, Eur. J. Solid State Inorg. Chem. 28 (1991) 441–451.
[33] Q. Zhou, L. Dolgov, A.M. Srivastava, L. Zhou, Z.L. Wang, J.X. Shi, M.D. Dramićanin, M.G. Brik, M.M. Wu, $Mn^{2+}$ and $Mn^{4+}$ red phosphors: synthesis, luminescence and applications in WLEDs. A review, J. Mater. Chem. C 6 (2018) 2652–2671.
[34] M.G. Brik, A.M. Srivastava, N.M. Avram, Comparative analysis of crystal field effects and energy level scheme of six-fold coordinated $Cr^{4+}$ ion in the pyrochlores, $Y_2B_2O_7$ ($B = Ti^{4+}$, $Sn^{4+}$), J. Lumin. 131 (2011) 54–58.
[35] A.M. Srivastava, M.G. Brik, Ab initio and crystal field studies of the $Mn^{4+}$-doped $Ba_2LaNbO_6$ double-perovskite, J. Lumin. 132 (2012) 579–584.
[36] M.G. Brik, A.M. Srivastava, A computation study of site occupancy in the commercial $Mg_{28}Ge_{7.55}O_{32}F_{15.04}:Mn^{4+}$ phosphor, Opt. Mater. 54 (2016) 245–251.
[37] M.G. Brik, A.M. Srivastava, Comparative crystal field analysis of energy level schemes and nephelauxetic effect for $Cr^{4+}$, $Cr^{3+}$, and $Mn^{4+}$ ions in $Y_2Sn_2O_7$ pyrochlore, Opt. Mater. 35 (2013) 1251–1256.
[38] M.Y. Peng, X.W. Yin, P.A. Tanner, M.G. Brik, P.F. Li, Site occupancy preference, enhancement mechanism, and thermal resistance of $Mn^{4+}$ red luminescence in $Sr_4Al_{14}O_{25}:Mn^{4+}$ for warm WLEDs, Chem. Mater. 27 (2015) 2938–2945.
[39] H. Egami, T. Oguma, T. Katsuki, Oxidation catalysis of Nb(salan) complexes: asymmetric epoxidation of allylic alcohols using aqueous hydrogen peroxide as an oxidant, J. Am. Chem. Soc. 132 (2010) 5886–5895.
[40] V. Parvulescu, C. Anastasescu, C. Constantin, B.L. Su, Mono (V, Nb) or bimetallic (V-Ti, Nb-Ti) ions modified MCM-41 catalysts: synthesis, characterization and catalysis in oxidation of hydrocarbons (aromatics and alcohols), Catal. Today 78 (2003) 477–485.
[41] S. Hayashi, N. Sasaki, S. Yamazoe, T. Tsukuda, Superior base catalysis of group 5 hexametalates $[M_6O_{19}]^8$ (M = Ta, Nb) over group 6 hexametalates $[M_6O_{19}]^2$ (M = Mo, W), J. Phys. Chem. C 122 (2018) 29398–29404.
[42] J.H. Li, Q.Y. Liang, J.Y. Hong, J. Yan, L. Dolgov, Y.Y. Meng, Y.Q. Xu, J.X. Shi, M.M. Wu, White light emission and enhanced color stability in a single-component host, ACS Appl. Mater. Interfaces 10 (2018) 18066–18072.
[43] L. Huang, Y.W. Zhu, X.J. Zhang, R. Zou, F.J. Pan, J. Wang, M.M. Wu, HF-free hydrothermal route for synthesis of highly efficient narrow-band red emitting phosphor $K_2Si_{1-x}F_6:xMn^{4+}$ for warm white light-emitting diodes, Chem. Mater. 8 (2016) 1495–1502.